# Tracer dynamics in a flow of driven vortices

A. Witt,[1] R. Braun,[1] F. Feudel,[1,2] Celso Grebogi,[2] and J. Kurths[1]
[1]*Institut für Physik, Universität Potsdam, Postfach 601553, D-14415 Potsdam, Germany*
[2]*Institute for Plasma Research, University of Maryland, College Park, Maryland 20742*
(Received 14 July 1998)

From numerical computations of the two-dimensional Navier-Stokes equations, we derive a low-dimensional stream-function model that captures the essential properties of the dynamics of an array of driven vortices in time-periodic regime. Using this analytical model, we study the Lagrangian dynamics of passive tracers and show that it is essentially controlled by the existence of a chaotic saddle. We obtain its stable and unstable manifolds, which in turn, yield an approximation of the chaotic saddle in terms of their intersections. By introducing symbolic dynamics, the spatiotemporal properties of the flow, including an alternative approximation of the chaotic saddle, are described in terms of measures of complexity. [S1063-651X(99)03102-5]

PACS number(s): 05.45.−a, 47.54.+r, 47.52.+j

## I. INTRODUCTION

Lagrangian dynamics is an alternative method of describing fluid dynamics in terms of Lagrangian coordinates through the motion of scalar tracers determined by the fluid velocity field. In addition to its practical applications such as the spread of pollutants in the atmosphere and in the oceans [1], it also provides an alternative view on pattern formation in hydrodynamical systems. Since the publication of the seminal paper by Aref [2], it has been realized that for simple time periodic flows the pathlines of tracer particles can already have a very complicated, intertwined, and chaotic shape, a phenomenon termed as Lagrangian turbulence. A comprehensive introduction on the topic of Lagrangian dynamics and mixing theory can be found in the book by Ottino [3], while an overview on recent research activities can be found in Ref. [4]. For incompressible fluids, especially for the two-dimensional case, there exists an exhaustive theory in terms of turnstyles and lobes leading to a deep understanding of the mixing phenomena [5].

The objective of the present paper is to apply methods of nonlinear dynamics to study the chaotic motion of passive tracers in the mixing region of a two-dimensional array of vortices. The simple fluid model used here is motivated by experiments performed in Refs. [6–9] and by numerical investigations on the two-dimensional Navier-Stokes equations [10,11]. In those experiments, the transition to turbulence in a linear chain of electrically driven vortices was studied. By increasing the Reynolds number, which was controlled by the strength of the applied current, variation in the spatial structure and temporal evolution of the flow was explored.

From numerical simulations of the two-dimensional Navier-Stokes equations, we find strong evidence that the essential dynamics, at least for moderate Reynolds numbers, can be captured by a low-dimensional model. It consists of a five-mode approximation and it gives the basic features of the first bifurcating solution branches. We prescribe the stream-function in form of this five-mode approximation to model the driven flow of vortices, and study the Lagrangian dynamics by applying an external time-periodic pertubation. This model is used to emulate the dynamics of the vortex flow beyond the Hopf bifurcation as the Reynolds number is increased. The resulting flow consists of a shear component and a chain of corotating vortices both varying periodically in time. A blob of passive tracers injected into the fluid in the region between the vortices and the shear flow acquires a rather irregular and chaotic dynamics. The separatrices of the unperturbed flow then break off producing a separating layer in which the chaotic motion takes place. In this paper, we argue that an invariant chaotic saddle and its stable and unstable manifolds, control the essential dynamics in this layer.

Chaotic saddles play a fundamental role in dynamical systems, especially in Hamiltonian systems, where the phase volume is conserved. They are invariant sets under the dynamics and they strongly influence the qualitative behavior of the whole solution structure. The presence of chaotic saddles in the Lagrangian dynamics of open hydrodynamical flows has been shown by means of an analytical stream-function model for the von Kármán vortex street by Péntek *et al.* [12]. They demonstrated that the chaotic saddle is responsible for the mixing property and chaotic behavior of the particle advection. The evolution of two adjacent dyes reveals the fractal nature of their common boundary, and that is a signature for the existence of a chaotic saddle in the dynamics. Moreover, this boundary exhibits such peculiar features as the Wada property [13].

Our objective here is to reveal the existence of chaotic saddles in closed hydrodynamical flow of vortices, driven periodically in time. By contrast to open hydrodynamical flows, as considered in Refs. [12,13], asymptotic stationary states of tracer trajectories does not apply here in the infinite time limit ($t \rightarrow \pm\infty$) and therefore scattering techniques cannot be used. We then apply the concept of symbolic dynamics and introduce special measures of complexity [14–16] in order to expose the nature of the chaotic saddle and to display its stable and unstable manifolds.

In Sec. II, we review briefly the bifurcations in a flow of driven vortices as determined by the Navier-Stokes equations. From these results, a low-dimensional stream-function model is derived that we use to study the Lagrangian dynamics. Then, in Sec. III, we elucidate the internal structure of the chaotic mixing layer by approximating the structure of the stable and unstable manifolds of a chaotic saddle. In Sec. IV, techniques from symbolic dynamics are introduced to

 

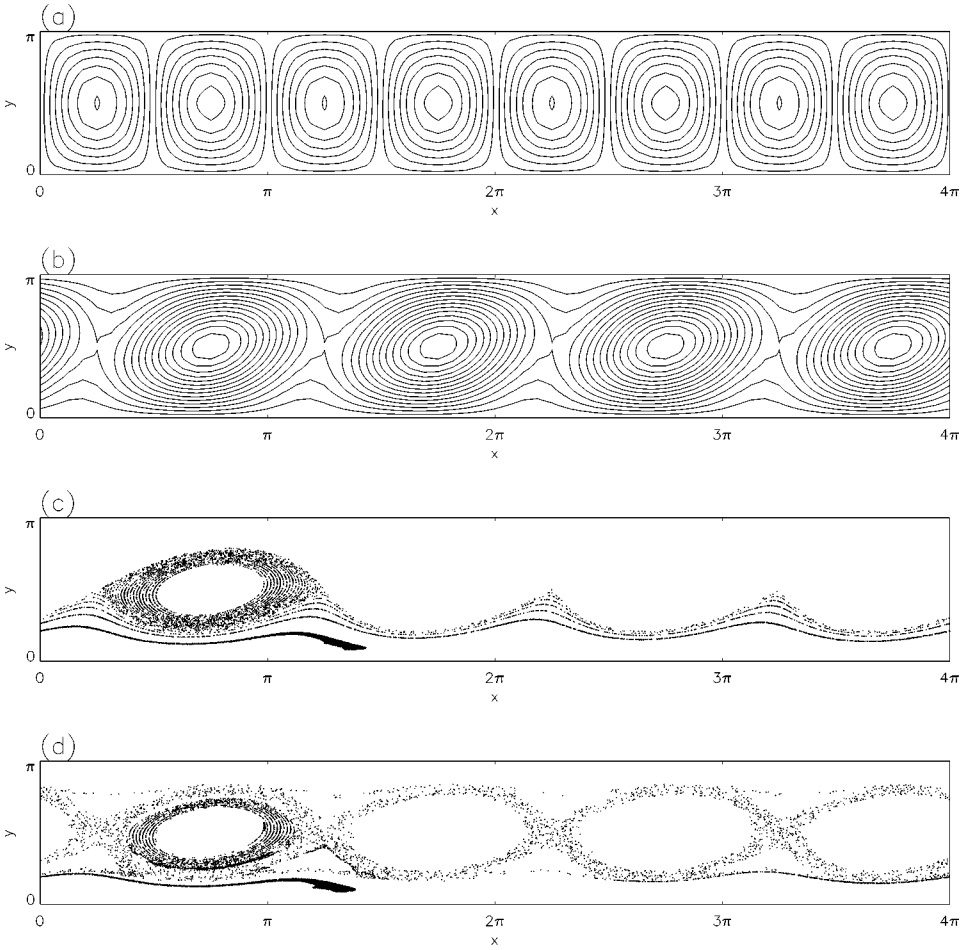


FIG. 1. Streamlines of (a) eight driven counter-rotating vortices ($f=26.7$) and (b) corotating vortices beyond the first pitchfork bifurcation ($f=43.3$). Lagrangian dynamics of passive tracers injected in (c) a steady state flow and in (d) a time-periodically varying flow.

study the invariant dynamics of tracers. Finally, in Sec. V, conclusions are given.

## II. STREAMLINE MODEL OF THE DRIVEN VORTICES

Our investigations are motivated by fluid experiments, see Refs. [6–9], using electrolytic solutions. The Lorentz force, resulting from an applied current flowing through the electrolyte, drives a chain of counter-rotating vortices. This experiment can be modeled by two-dimensional Navier-Stokes equations with an external forcing in the form of

$$\frac{\partial \boldsymbol{v}}{\partial t}+(\boldsymbol{v}\cdot\boldsymbol{\nabla})\boldsymbol{v}=\nabla^2\boldsymbol{v}-\boldsymbol{\nabla}p+\boldsymbol{f}, \tag{1}$$

$$\boldsymbol{\nabla}\cdot\boldsymbol{v}=0, \tag{2}$$

where $\boldsymbol{v}$ is the fluid velocity field, $p$ is the thermal pressure, and $\boldsymbol{f}$ represents the external force chosen to be

$$\boldsymbol{f}=f\begin{pmatrix}\sin k_1 x\cos k_2 y\\ -\cos k_1 x\sin k_2 y\end{pmatrix}. \tag{3}$$

By fixing the two constants $k_1$ and $k_2$ at $k_1=2$ and $k_2=1$, we get an array of eight counter-rotating eddies in the region $\Omega=[0,4\pi]\times[0,\pi]$. The scalar parameter $f$ stands for the strength of the Lorentz force and it is in turn quantitatively related to the Reynolds number. For a weak forcing, corresponding to small Raynolds numbers, the array of eight counter-rotating vortices [see Fig. 1(a)] is the only time-asymptotic state. Increasing the strength of the forcing, this primary steady state loses its stability and a sequence of further bifurcations, ending up in chaos, is produced. A detailed bifurcation analysis of the scenario has been described in Refs. [17,18]. We review those bifurcations only thus far as

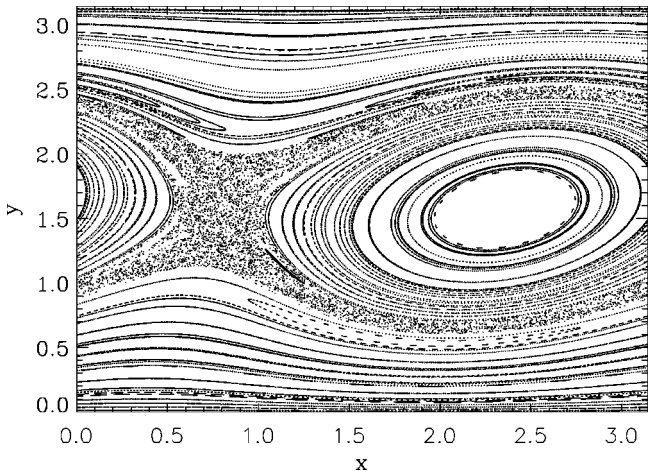


FIG. 2. Stroboscopic map of particle dynamics in the region of the first vortex.

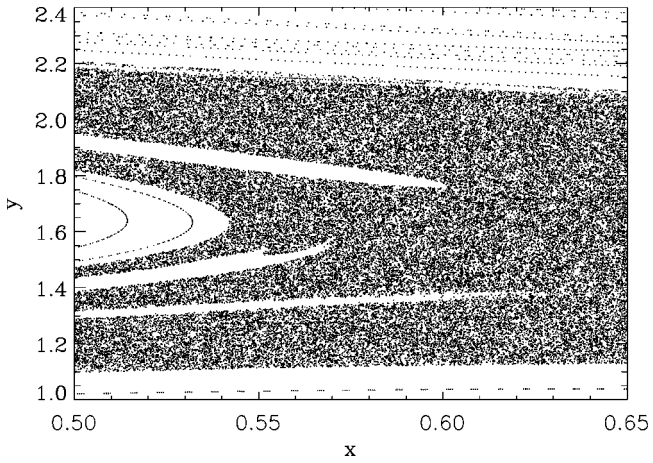


FIG. 3. Surviving KAM tori in an enlargement of Fig. 2.

it is necessary to derive the stream-line model that we use to study the Lagrangian dynamics.

At a critical Reynolds number the primary solution branch bifurcates in a secondary steady state consisting of four corotating vortices and a shear component [see Fig. 1(b)]. They are separated by heteroclinic lines connecting the hyperbolic fixed points of the flow. A second pitchfork bifurcation changes the streamline portrait only slightly. The resulting stationary branch is stable within only a very small interval of the forcing parameter, and eventually, it loses stability in a Hopf bifurcation. We have neglected this intermediate steady-state branch and set up a model which reflects the essence of the secondary steady states and the proceeding time-periodic dynamics of the velocity field after the Hopf bifurcation.

A detailed inspection of the secondary steady states gives evidence that five modes are sufficient to capture more than 99% of the entire vorticity of the flow. These five modes provide a good approximation of the spatial flow structure. Thus, using the stream-function formulation, the flow can be approximated by

$$\psi(x,y)=\psi_1\sin(y)+\psi_2\sin(3y)+\psi_3\sin(2x)\sin(y)+\psi_4\cos(2x)\sin(2y)+\psi_5\sin(2x)\sin(3y). \quad (4)$$

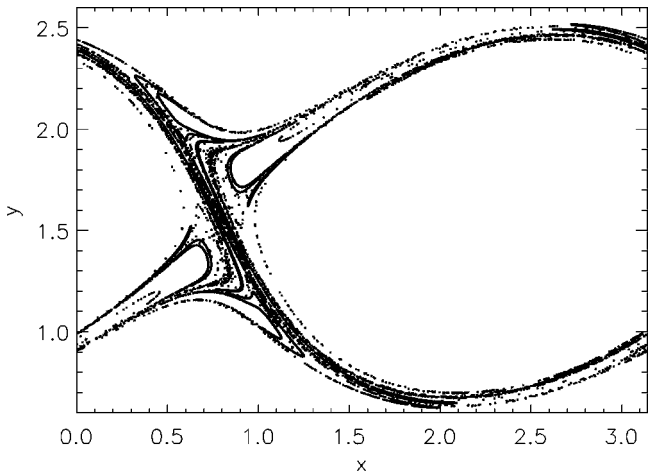


FIG. 4. Approximation of the unstable manifolds by the evolution of passive tracers that are injected as a blob at one of the hyperbolic fixed points of the original steady state.

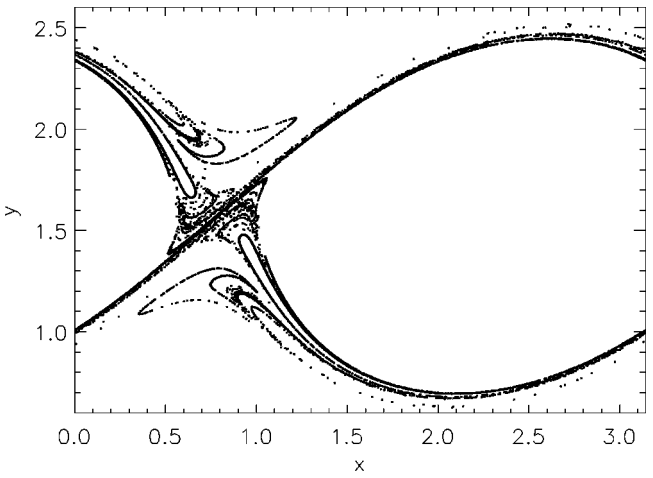


FIG. 5. Approximation of the stable manifolds as in Fig. 4 by reversing the integration time.

The coefficients $\psi_1$ and $\psi_2$ measure the strength of the shear flow component, $\psi_3$ represents the original eight-vortex forcing, and $\psi_4$ and $\psi_5$ are responsible for the tilting of the eddies [see Fig. 1(b)]. The concrete form of the time dependence, which we introduce in the stream-function model, is motivated by two features suggested by Navier-Stokes simulations. First, the spatial structure of the velocity field is only slightly modulated by the time dependence, even in the chaotic regime. Secondly, the time scales of these variations are typically larger than the turnover time, that is, the time a passive tracer needs to move once around a vortex. The turnover time is the characteristic time scale which we set to be of the order of 1. We vary all the coefficients of the modes in Eq. (4) periodically as

$$\psi_i(t)=\psi_i[1+\delta\sin(\omega_1 t)], \quad (5)$$

where $\delta$ is a constant that measures the strength of the modulation. Fixing the coefficients $\psi_i$ by values that we get from the dominating modes in the Navier-Stokes simulations, Eq. (4) reproduces qualitatively the same streamlines as the Navier-Stokes flow in Fig. 1(b).

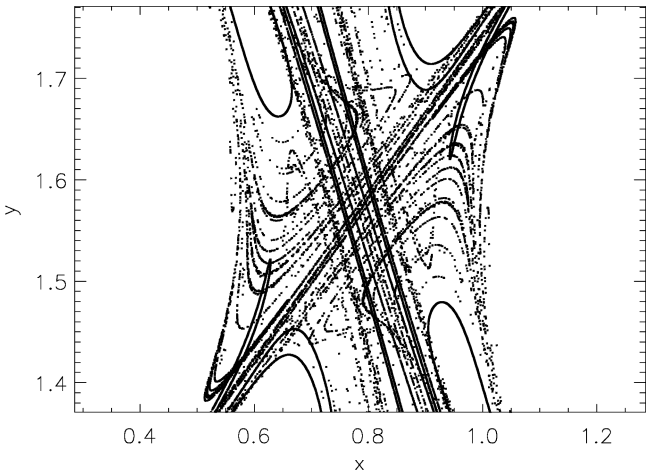


FIG. 6. Intersection of stable and unstable manifolds in an enlargement of Figs. 4 and 5.

Proceeding now with investigations of the Lagrangian dynamics, we specify the flow by our analytical streamfunction model Eq. (4) and obtain a nonsteady dynamics of the velocity field by varying the coefficients $\psi_i$ periodically according to Eq. (5) with $\delta$ chosen to be $\delta=0.2$. Figure 1(c) shows the Lagrangian dynamics of tracers in the steady-state flow governed by the velocity field of corotating vortices that is exhibited in Fig. 1(b). In practice, we inject a square dye of 10 000 tracers placed in the lower region of the left most vortex, where the heteroclinic line separates the vortex from the shear flow. The particles located inside the vortex wrapup around its center and are trapped forever. The other particles follow the shear flow, with slow speed in the neighborhood of the separatrices and with higher speed in the tonguelike blobs far from the vortices. We use periodic boundary conditions in the horizontal direction and, as a result, the particles escaping at the right side of Fig. 1(c) reappear on the left side. Due to the steady-state character of the velocity field, the region of the other vortices are separated and particles cannot enter them. However, when the flow gets a time dependence, the particle dynamics is much more complicated. Figure 1(d) shows the spread of passive tracers, initialized as previously, but now for a simulation having a time-periodic flow. The hyperbolic fixed points of the steady flow become hyperbolic fixed points in the Poincaré section. Their stable and unstable manifolds intersect heteroclinically forming heteroclinic tangles which are responsible for the chaotic advection near the vortices. Typically, a particle in the layer about a vortex moves in its neighborhood for an indefinite period until it switches randomly to one of the neighboring vortices. The rough shape of the chaotic layer can be seen in Fig. 1(d) but the details of its structure are not discernible. In the following we analyze the fine structure of the layer in more detail and explain the mechanism producing the irregular motion of tracers in terms of chaotic saddles.

## III. INTERNAL STRUCTURE OF THE CHAOTIC LAYER

Because of the incompressibility of the velocity field the equations for the tracers, given in the streamline formulation by

$$\dot{x}=\frac{\partial\psi}{\partial y}, \quad \dot{y}=-\frac{\partial\psi}{\partial x}, \tag{6}$$

constitute a Hamiltonian system, generally depending on time. We study its dynamics for a set of tracers in the time-periodic situation governed by Eqs. (4), (5).

Stroboscopic maps offer a standard technique for visualizing the dynamics of periodically driven systems. The trajectories are mapped on the Poincaré section by sampling them at multiple times of the driving period. The stroboscopic map for the Lagrangian dynamics of a set of passive tracer particles, moving in the array of vortices, is presented in Fig. 2. The periodic motion near the center of a vortex is represented by closed loops in the case of irrational ratio between the forcing period and the orbit time, for rational ratio they degenerate into a finite set of points. Similarly, the regular motion in the shear part of the flow is also mirrored by smooth lines.

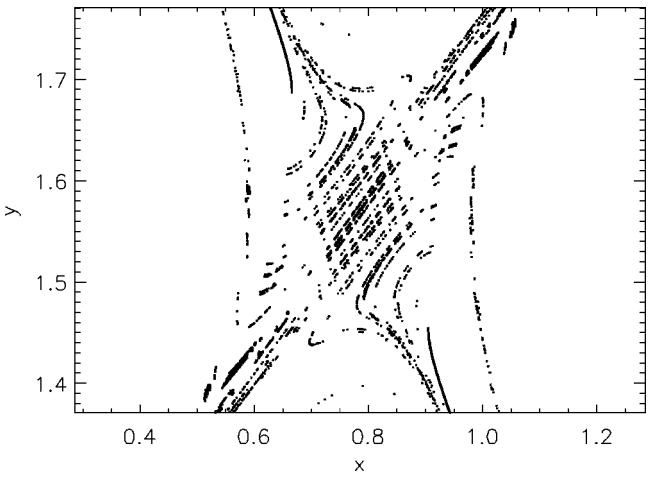


FIG. 7. The chaotic saddle is approximated by the intersecting points of the stable and unstable manifolds.

More interesting is the irregular motion in the layer between the vortices and the shear flow. In this layer the particles move nonperiodically, i.e., in the stroboscopic map no regular structure such as a line or a loop is visible. Due to the Hamiltonian characteristic of the system, each particle starting in the layer covers during its time evolution the complete layer. However, this layer is interspersed by infinitely many surviving KAM tori, i.e., the layer has holes and it is therefore structured similar to a sponge. The particle motion in those holes is regular again but not as simple as inside the vortices or in the shear flow. Their quasiperiodic dynamics is caused by a higher frequency ratio. In a blow-up of the layer, as shown in Fig. 3, some of the surviving KAM tori are discernible.

In the Poincaré section the layer resembles Swiss cheese with KAM tori as holes but without other internal structures. However, the evolution of passive tracers injected into this region produces patterns which look similar to fractal objects. The presence of a chaotic saddle, together with its stable and unstable manifolds, is responsible for this intricate structure formation. A chaotic saddle is an invariant set at the intersection of the closure of its stable and unstable manifolds. The sprinkling of tracer particles in the chaotic saddle region is a standard technique to visualize and approximate the unstable manifolds [19]. The tracers are placed as a small ball about one of the hyperbolic fixed points that exist in the original steady state and where the saddle is located. Figure 4 shows the nearly quasistationary distribution of tracers after a long integration time. The stable manifolds can be approximated by the same procedure by reversing the integration time as shown in Fig. 5. The composition of both figures in a blow-up region about the saddle is shown in Fig. 6. Eventually, Fig. 7 yields an approximation for the chaotic saddle retaining only those points of Fig. 6 which approximate the intersection of both manifolds. It should be mentioned that the chaotic saddle as an invariant set consists of course of all the copies generated by the symmetry transformations of the flow.

## IV. SYMBOLIC DYNAMICS

Techniques of symbolic dynamics are well-developed in the case of maps with a single critical point [14,15,20]. For

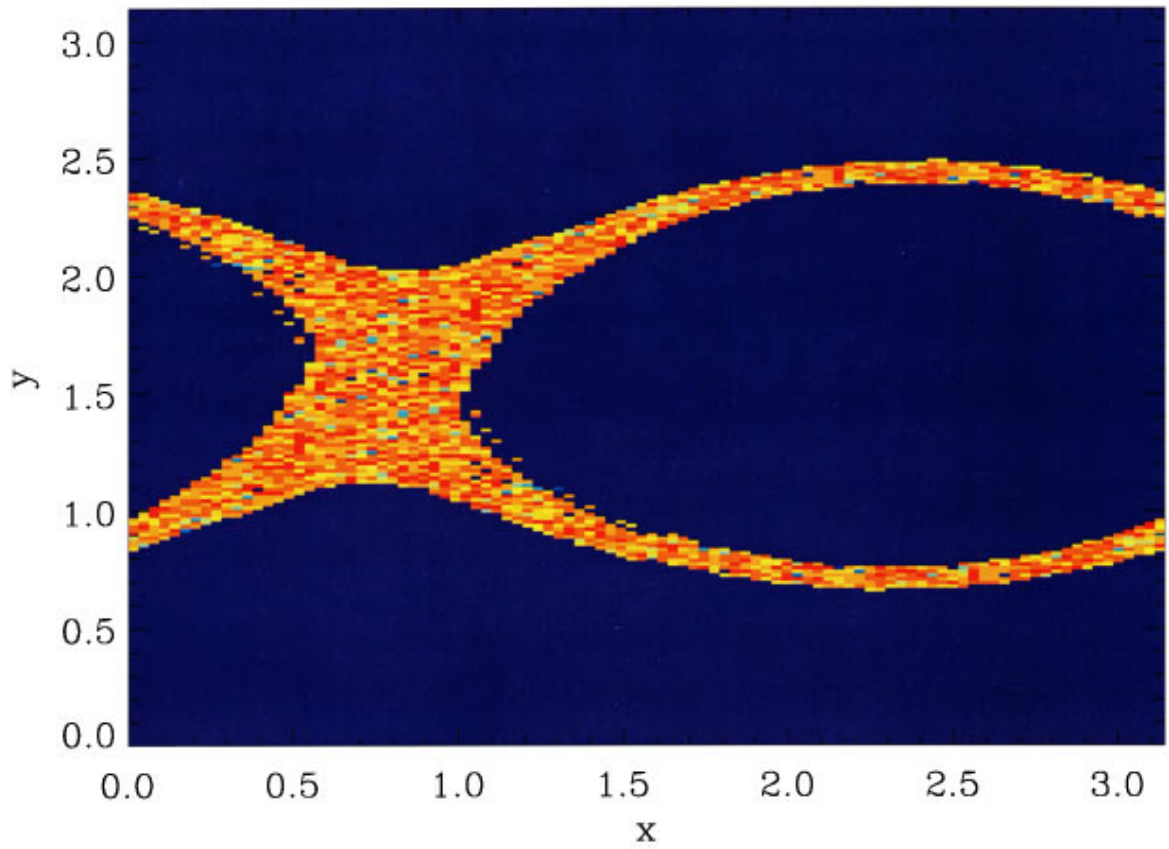


FIG. 8. (Color) Shannon entropy of particle dynamics in the region of the left most vortex. The light colors indicate positive values of the Shannon entropy suggesting the irregularity of the particle motion in the chaotic layer.

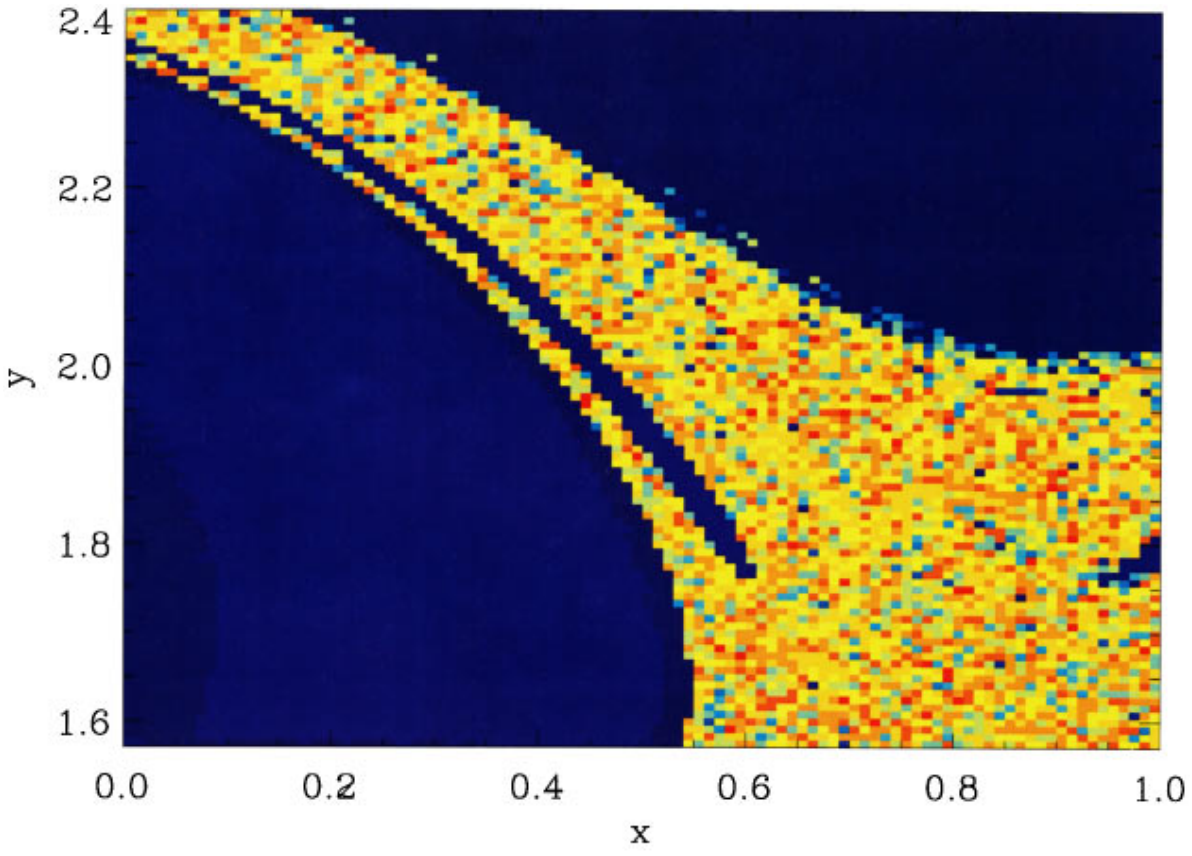


FIG. 9. (Color) Shannon entropy in an enlargement of Fig. 8.

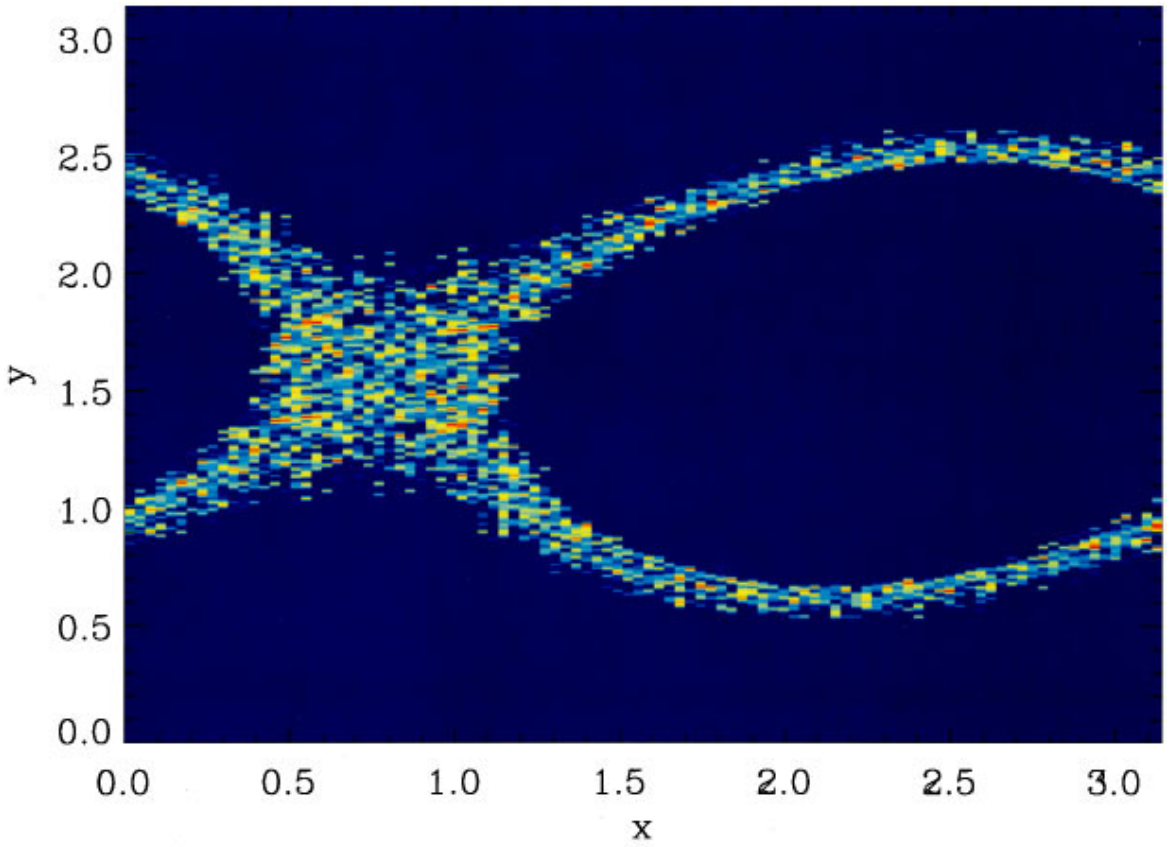


FIG. 10. (Color) Shannon entropy of a system for which the velocity field is changing chaotically in time.

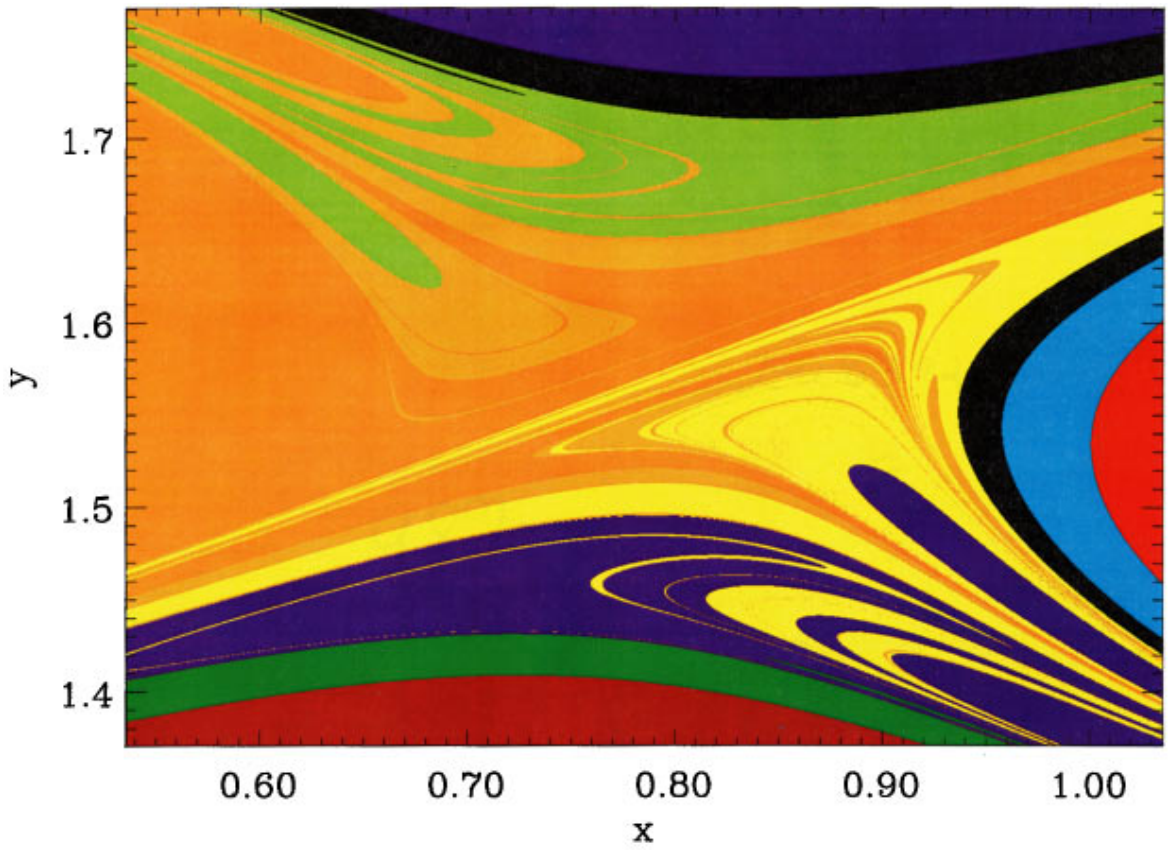


FIG. 11. (Color) Partition $\mathcal{A}_l$ for $l=14$.

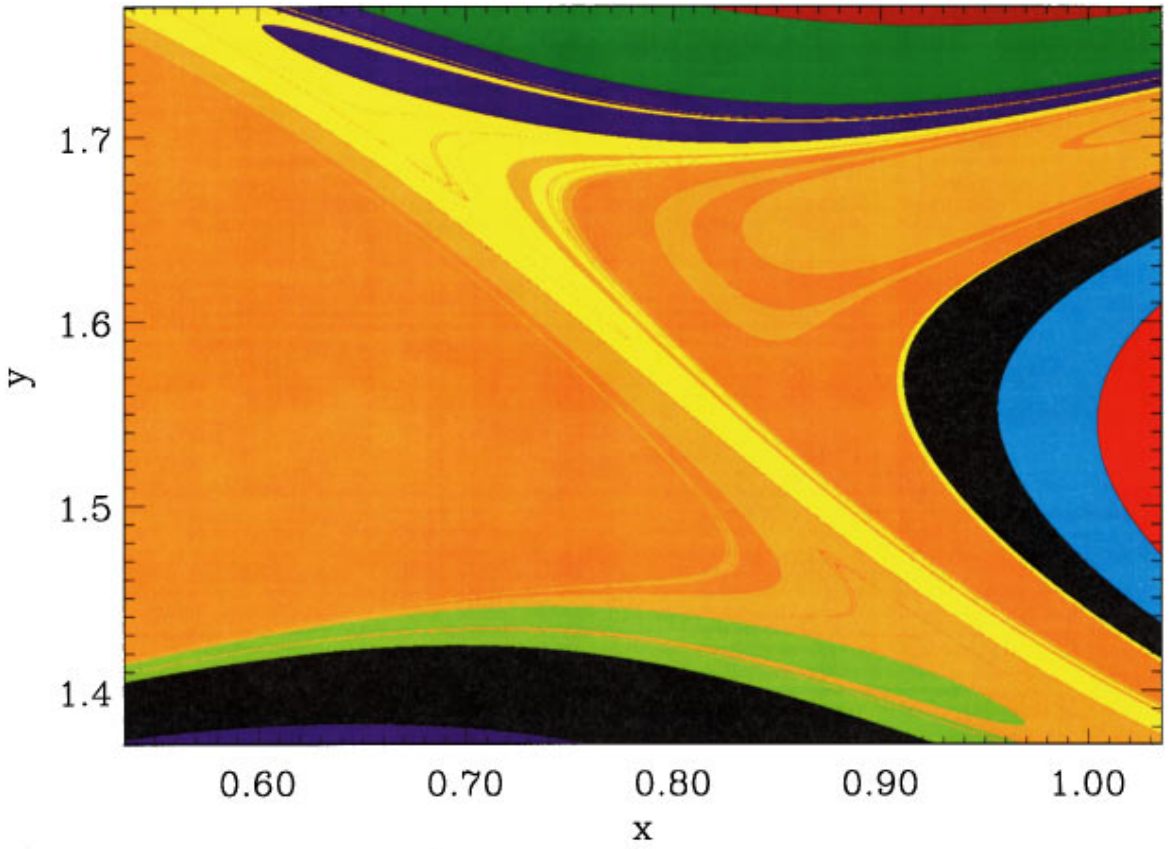


FIG. 12. (Color) Partition $\mathcal{A}_l^-$ for $l=14$.

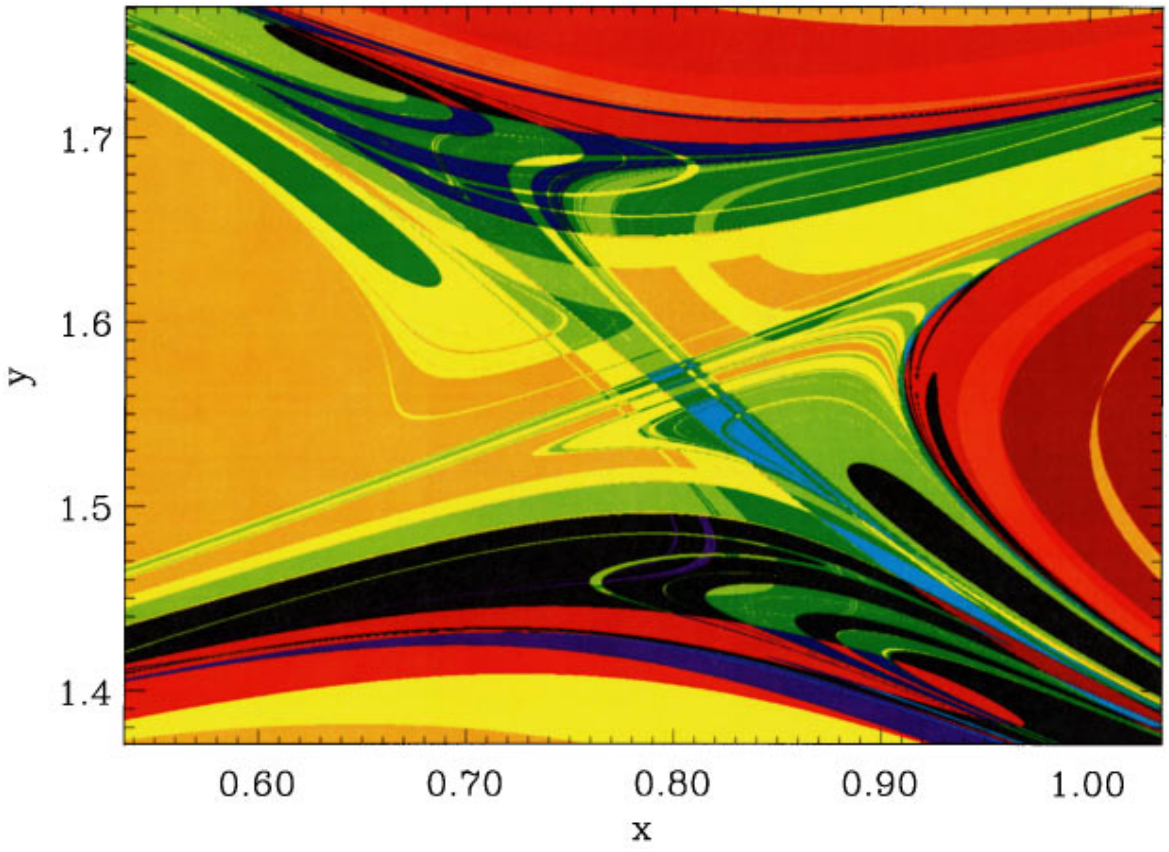


FIG. 13. (Color) Intersection of the stable and unstable manifold yields an approximation of the chaotic saddle.

this rather simple family, generating partitions are known to exist enabling an efficient coding of the dynamics in terms of symbol sequences, and thus keeping the complete information of the system in its symbolic dynamics. This property is expressed in the coincidence of the Shannon entropy of the symbol sequence with the Kolmogorov-Sinai entropy of the system and, consequently, with the sum of the largest Lyapunov exponents.

The dynamics of low-dimensional systems can be analyzed by using symbolic dynamics if Poincaré maps are introduced [21,22]. On the other hand, higher-dimensional maps are rarely studied by means of symbolic dynamics, since generating partitions are difficult to find [19]. Nevertheless, the applications of this concept even to data from complex natural systems (e.g., earth magnetic field [23], human cardiac systems [24], or cognitive complexity [25]) or to nonlinear stochastic systems [26] efficiently exhibits insights into the underlying dynamics.

The characterization of the symbol sequences is not restricted to the estimate of Shannon entropy. A broad range of so-called measures of complexity [16] allows a more detailed characterization of the structure of these symbol sequences. Further there have been several attempts to find the grammatical rules of the symbolic dynamics [27].

For the model under study, we first need a transformation from the state space $(x(t),y(t))$ to a symbol space by discretizing space and time. The idea is to find a map of the trajectories into the set of symbol sequences such that regular motions, as given by the tracers in the shear flow or by their long lasting circulation inside the vortices, have also regular symbol sequences. In order to keep the computational requirements as small as possible, we look for effective transformations into symbol sequences with a minimal number of different symbols. We attempt to work only with three symbols denoted by $s_i \in \{-1,0,1\}$. Furthermore, we divide the domain $\Omega=[0,4\pi]\times[0,\pi]$ in four cells by cuts along vertical lines that are placed on the vortex centers. In other words, a cell consists of two halves of neighboring vortices and the separating region in between. At all times, when the tracer leaves a cell, i.e., when it intersects the $x$ coordinate of some vortex center, a symbol $s_i$ is produced. We choose the rule to assign a 0 if the tracer reenters into the same cell that it has left in the previous step. Obviously, this event accords to a continuing circulation about one of the vortices. If the tracer goes accross the entire cell from left to right or in the reversal direction we allot the symbol 1 or $-1$, respectively, at the instant when the tracer leaves the cell. This situation accounts for the motion governed by the shear flow.

Since an attractor does not exist here, one has to study the structure of the symbol sequences with relation to the initial conditions $x_0$. Initial conditions near the centers of the vortices generate symbol sequences containing only zeros, i.e., $\mathcal{S}=(000\ldots)$. If the tracer is starting in the shear part of the flow, the symbol sequence is constant. By starting in the lower shear flow, all the symbols are equal to 1 and by starting in the upper one, the corresponding symbol sequence contains only $-1$. For initial conditions in the layer, more complicated symbol sequences appear; they contain the three basic symbols in an aperiodic sequence. Due to the ergodicity of the particles in the layer, all tracers starting there generate equally structured symbol sequences. The special properties of these symbol sequences are discussed in the next subsections.

### A. Shannon entropy

The traditional quantity for characterizing a symbol sequence is the Shannon entropy [28]. The Shannon entropy of $n$th order $H_n$ is based on the probability distribution of length-$n$ substrings $s^n$ (words of length $n$) of the symbol sequence

$$H_n=-\sum_{s^n\in A^n, p(s^n)>0} p(s^n)\log_2 p(s^n), \tag{7}$$

where $A^n$ denotes the set of all possible length-$n$ words. $H_n$ measures the average number of bits needed to specify an arbitrary word of length $n$ in a sequence $S$. Their differences

$$h_n=H_{n+1}-H_n, \tag{8}$$

$$h_0=H_1, \tag{9}$$

quantify the information needed to determine the $(n+1)$th symbol of an arbitrary word of a given sequence if the first $n$ symbols are known. Already the sequence of $\{h_i\}$ is monotonically decreasing. The Shannon entropy of the system is then defined as the limit of $h_n$

$$h=\lim_{n\to\infty} h_n. \tag{10}$$

It describes the mean information contents per symbol. For the $h_n$ the following holds.

(1) For period-$p$ sequences, all $h_n$ with $n\geqslant p$ vanish.

(2) Due to Eqs. (7) and (8), all $h_n$ are equal to $h_0$ in case of purely random symbol sequences (white noise).

(3) For $k$th order Markov processes, the entropy differences reach the Shannon entropy of the system for $n=k$: $h_n=h$ for $n>k$. In the general case of more complicated sequences, the $h_k$ converge asymptotically to the limit $h$.

The Shannon entropy is a measure of randomness in the sense that it reaches its maximum in case of completely uncorrelated symbol chains. Due to the passage to the limit in the definition of Shannon entropy, its numerical computation turns out to be difficult. To bypass this problem, we approximate the Shannon entropy in the following by the Lempel-Ziv complexity [29–31].

Our objective in considering the Shannon entropy is to characterize the dynamical nature of the tracer motion. We attempt to explore the information encoded in the symbolic sequences with the aim to distinguish spatial regions with different Lagrangian dynamics. The Shannon entropy was calculated for a set of tracers initially placed on a grid consisting of $100\times100$ grid points. The results are presented in Figs. 8 and 9. Dark regions are related to vanishing Shannon entropy, lighter colors mean larger positive values. One finds, as expected, larger positive entropy for tracers starting on the layer, and vanishing small values for all other initial conditions. In the blowup as shown in Fig. 9 even the regular regions of the surviving KAM tori in the layer are discernible. Furthermore, the Shannon entropies for tracers moving

in the layer are approximately of the same size, a feature that indicates the ergodic character of the Lagrangian dynamics in this region.

These computations confirm the results obtained using stroboscopic maps. But additionally, we attempt to apply this approach also to more general situations in which the technique of stroboscopic maps fails. They are, for instance, the Lagrangian dynamics governed by a velocity field varying quasiperiodically or chaotically in time. As an example, we show in Fig. 10 the Shannon entropy computed for a system in which the coefficients $\psi_i$ in Eq. (4) are chaotically modulated in time by the $x$ coordinate of the Lorenz system. The rough shape of the layer is the same as in case of the periodic modulation (see Fig. 8), whereas its fine structure appears to be more filigree.

### B. Chaotic saddles

In this subsection we return to the periodic time dependence of the flow and we show that the introduction of symbolic dynamics gives an alternative technique in approximating the chaotic saddle. We proceed to approximate it in the following manner. For a dense grid of initial conditions the short-time symbolic dynamics is computed, i.e., for each point on the grid the first $l$ symbols are obtained. Furthermore, the $[0,\pi]\times[0,4\pi]$ plane is partitioned into cells which contain initial conditions leading to the same symbolic dynamics with respect to the first $l$ symbols. We call this partition $\mathcal{A}_l$, and its cells $A_i$, $i=1,\ldots,n_l$. By construction, each cell $A_i$ is related to a single word of length $l$, the volume of this cell is equal to the probability of the word in the system under random initial condition. Due to positive Shannon entropy, the number of words is increasing exponentially with the word length $l$ just as the number of cells. Since the symbol sequences near the centers of the vortices and near the boundary are constant, new cells are only created on the chaotic layer.

The set $\partial\mathcal{A}_l$, which contains the boundaries of all cells of the partition $\mathcal{A}_l$, consists of nonintersecting curves. The unstable periodic orbits (fixed points in the Poincare section), which are produced from the hyperbolic fixed points of the original steady state flow by the periodic modulation in time, belong to $\partial\mathcal{A}_l$. The set $\partial\mathcal{A}_l$ grows as the number $l$ of the first relevant symbols determining the partition $\mathcal{A}_l$ increases, $\partial\mathcal{A}_{l-1}\subset\partial\mathcal{A}_l$. Similarly, both the number of cells $\mathcal{A}_l$ and the boundary set $\partial\mathcal{A}_l$ grows exponentially. Due to the irregular nature of the motion in the layer, including stretching and folding properties of volume elements, this procedure leads to longer and longer line elements in $\partial\mathcal{A}_l$. Finally, we obtain a limit set $\partial\mathcal{A}$ for $l\to\infty$. By construction this set $\partial\mathcal{A}$ forms the stable manifolds of the periodic orbits introduced above. The same procedure can be repeated for the backward dynamics and it yields the unstable manifolds.

In Fig. 11 the partition $\mathcal{A}_l$ for $l=14$ is displayed using different colors, their boundaries are an approximation of the stable manifolds. Analogously, in Fig. 12, the partition $\mathcal{A}_l^-$ $(l=14)$ and their boundaries represent the unstable manifolds. As discussed, the intersections of the stable and unstable manifolds forms the approximation of the chaotic saddle, which basically controls the dynamics in the considered system. In Fig. 13, we give an indication of this set by an overlap of $\mathcal{A}_l$ and $\mathcal{A}_l^-$.

## V. CONCLUDING REMARKS

In this paper, we have studied the chaotic motion of tracers in a chain of driven vortices introducing an analytical model which we have derived by numerical simulations of the orginal Navier-Stokes equations. Using this model we have given evidence for the existence of a chaotic saddle controlling the Lagrangian dynamics in this closed Hamiltonian system. In addition to presenting approximations of the stable and unstable manifolds of the chaotic saddle, we have introduced methods from symbolic dynamics to characterize the dynamics of tracers in a temporally varying flow. In doing so, we have recovered the structure of stable and unstable manifolds of the chaotic saddle and thus verifying the viability of our alternative method. These techniques of symbolic dynamics can also be extended to attack the problem of particle dynamics in fluids with more general time dependences such as, for instance, quasiperiodic, chaotic, or stochastic properties.

## ACKNOWLEDGMENTS

F.F. thanks the University of Maryland for its hospitality during his stay. A. Witt was supported by Verein Deutscher Ingenieure (Grant No. 13N7000/7), and by the Max-Planck-Gesellschaft. This work was also supported by the U.S. Department of Energy (Mathematical, Information and Computational Sciences Division, High Performance Computing and Communication Program).

[1] J. Holton *et al.*, Rev. Geophys. **33**, 403 (1995).
[2] H. Aref, J. Fluid Mech. **143**, 1 (1984).
[3] J. M. Ottino, *The Theory of Mixing: Stretching, Chaos and Transport* (Cambridge University Press, Cambridge, 1989).
[4] In *Chaos Applied to Fluid Mixing*, Vol. 4 of *Chaos, Solitons & Fractals*, edited by H. Aref (Pergamon, Oxford, 1994), pp. 745–1116.
[5] S. Wiggins, *Chaotic Transport in Dynamical Transport in Dynamical Systems* (Springer-Verlag, New York, 1992).
[6] P. Tabeling, B. Perrin, and S. Fauve, Europhys. Lett. **3**, 459 (1987).
[7] P. Tabeling, O. Cardoso, and B. Perrin, J. Fluid Mech. **213**, 511 (1990).
[8] O. Cardoso, H. Willaime, and P. Tabeling, Phys. Rev. Lett. **65**, 1869 (1990).
[9] H. Willaime, O. Cardoso, and P. Tabeling, Phys. Rev. E **48**, 288 (1993).
[10] J. M. Finn, J. F. Drake, and P. N. Guzdar, Phys. Fluids B **4**, 2758 (1992).
[11] P. N. Guzdar, J. M. Finn, A. V. Rogalsky, and J. F. Drake, Phys. Rev. E **49**, 2062 (1994).
[12] A. Péntek *et al.*, Phys. Rev. E **51**, 4076 (1995).

[13] Z. Toroczkai *et al.*, Physica A **239**, 235 (1997).
[14] B.-L. Hao, *Elementary Symbolic Dynamics and Chaos in Dissipative Systems* (World Scientific, Singapore, 1989).
[15] B.-L. Hao, Physica D **51**, 161 (1991).
[16] R. Wackerbauer *et al.*, Chaos Solitons Fractals **4**, 133 (1994).
[17] R. Braun, F. Feudel, and P. Guzdar, Phys. Rev. E **58**, 1927 (1998).
[18] R. Braun, Ph.D. thesis, University of Potsdam, 1997 (unpublished).
[19] P. Grassberger and P. Kantz, Phys. Lett. A **133**, 235 (1985).
[20] P. Collet and J.-P. Eckmann, *Iterated Maps of the Interval as Dynamical Systems* (Birkhäuser, Boston, 1980).
[21] A. Pikowsky, M. Zaks, U. Feudel, and J. Kurths, Phys. Rev. E **52**, 285 (1995).
[22] R. Wackerbauer, Phys. Rev. E **52**, 4745 (1995).
[23] A. Witt, J. Kurths, F. Krause, and K. Fischer, Geophys. Astrophys. Fluid Dyn. **77**, 79 (1994).
[24] J. Kurths *et al.*, Chaos **88**, 88 (1995).
[25] R. Engbert *et al.*, Phys. Rev. E **56**, 5823 (1997).
[26] A. Witt, A. Neimann, and J. Kurths, Phys. Rev. E **55**, 5050 (1997).
[27] R. Badii and A. Politi, *Complexity* (Cambridge University Press, Cambridge, 1997).
[28] C. Shannon and W. Weaver, *The Mathematical Theory of Communication* (University of Illinois Press, Urbana, 1949).
[29] A. Lempel and J. Ziv, IEEE Trans. Inf. Theory **22**, 75 (1976).
[30] A. Lempel and J. Ziv, IEEE Trans. Inf. Theory **24**, 530 (1976).
[31] F. Kaspar and H. Schuster, Phys. Rev. A **36**, 842 (1987).